A Thermogelling Organic-Inorganic Hybrid Hydrogel with Excellent Printability, Shape Fidelity and Cytocompatibility for 3D Bioprinting

Chen Hu,[†] Taufiq Ahmad,[‡] Malik Salman Haider,[†] Lukas Hahn,[†] Philipp Stahlhut,[‡] Jürgen Groll,[‡] and Robert Luxenhofer[†,§,*]

[†]Functional Polymer Materials, Chair for Advanced Materials Synthesis, Institute for Functional Materials and Biofabrication, Department of Chemistry and Pharmacy, Julius-Maximilians-University Würzburg, Röntgenring 11, 97070 Würzburg, Germany
[‡]Department of Functional Materials in Medicine and Dentistry, Institute for Functional Materials and Biofabrication and Bavarian Polymer Institute, Julius-Maximilians-University Würzburg, Pleicherwall 2, 97070 Würzburg, Germany
[§]Soft Matter Chemistry, Department of Chemistry and Helsinki Institute of Sustainability Science, Faculty of Science, University of Helsinki, PB 55, 00014 Helsinki, Finland

KEYWORDS: *poly(2-oxazoline), thermogelling, fugitive support, alginate, clay*

ABSTRACT: The development of 3D bioprinting technology highly depends upon the availability of suitable bioinks and biomaterial inks. In this study, an advanced hybrid hydrogel ink was developed, based on a poly(2-oxazoline)s/poly(2-oxazine)s diblock copolymer, alginate and clay i.e. Laponite XLG. The reversible thermogelling and shear thinning properties of the poly(2-oxazoline)-based diblock copolymer, acting as a fugitive material on the (macro)molecular level, facilitated the cell-laden extrusion based bioprinting process with high printability, shape fidelity and cell viability. Various three-dimensional constructs, including suspended filaments, were printed successfully with high shape fidelity and excellent stackability. Subsequent ionic crosslinking of alginate, fixates the printed scaffolds, which exhibit good mechanical stability, flexibility and structural integrity after extracting the fugitive print-support from the hydrogels by exhaustive washing. Finally, cell-laden printing and culture over 5 days demonstrated the cytocompatibility and feasibility of the novel hybrid hydrogels for 3D bioprinting. We believe that the developed material could be interesting for a wide range of bioprinting applications including tissue engineering and drug screening, potentially enabling also other biological bioinks such as collagen, hyaluronic acid, decellularized extracellular matrix or cellulose based bioinks.

INTRODUCTION

Additive manufacturing and extrusion-based 3D bioprinting have emerged as transformative technologies in tissue engineering and regenerative medicine to allow the rapid fabrication of customized complex 3D functional and cell-laden scaffolds.[1-5] Apart from the considerable attention focused on developing methods and strategies for 3D printing of materials, specialized biomaterials (i.e., (bio)inks) are a crucial component of any bioprinting technology.[6-10] Among the many biomaterials available, the natural polysaccharide alginate and its hydrogel is one of the most widely used material in 3D bioprinting.[11-13] Its tailorable degradation kinetics, ease of gelation, and favorable cyto- and biocompatibility that support cell survival and differentiation in culture are among its positive aspects. However, plain alginate formulations notoriously suffer from poor printability due to their limiting rheological properties. Therefore, many different approaches have been proposed to improve the rheological characteristics or printing methodology to enable "real" 3D printing of alginate based (bio)inks.[7, 14] For example, the printing of alginate or pre-/semi-crosslinked alginate/$CaCl_2$ ($CaCO_3$) in solutions or in the presence of small droplets (mist) containing $CaCl_2$,[15-17] the modification of commercially available 3D printer nozzles (coaxial nozzle-assisted system),[18-19] and the use of rheology modifiers such as clay,[20-21] graphene oxide,[22-23] and nanocellulose,[24-25] etc. have been proposed. In addition, support baths have been used to overcome the rheological limitations of alginate (bio)inks, and allow the fabrication of complex structures by providing an additional support for the ink during printing process.[26-27] Despite these advances, more advanced alginate-based (bio)inks that meet certain rheological properties and biological characteristics to realize the cell-friendly fabrication of complex 3D structures with high printability and shape fidelity while maintaining high cell viability and structural integrity during cultivation still represents a significant challenge for the bioprinting community.

Poly(2-oxazoline)s (POx) and poly(2-oxazine)s (POzi) are a diverse family of polymers easily accessible *via* living cationic ring opening polymerization

(LCROP).[28-30] In the last few decades, their synthesis has flourished, and come into the focus of biomaterials research as an alternative to the established PEG systems due to their pseudo-polypeptide structure, tunable physico-chemical versatility and cyto/biocompatibility.[31-35] Apart from many other biomedical applications, the recent developments on the thermogelling POx/POzi-based materials suggest their potential as 3D (bio)printable material.[36-38] In particular in 2017, Lorson *et al.* reported a thermogelling supramolecular hydrogel of a AB-type diblock copolymer comprising poly(2-methyl-2-oxazoline) (PMeOx) (A-block) and poly(2-*n*-propyl-2-oxazine) (PnPrOzi) (B-block) as a cytocompatible bioink for 3D bioprinting, but shape fidelity and stackability was not ideal for high-resolution 3D printing.[36] This could be significantly improved by addition of clay as rheological modifiers.[39] Very recently, Haider *et al.* introduced an alternative in with the PMeOx block was exchanged with an poly(2-ethyl-2-oxazoline).[40] However, the lacking long-term stability of the printed constructs remains a major drawback – upon addition of excess cell culture media necessary for longer-term cell culture, these constructs will simply dissolve. Hahn *et al.* reported on cytocompatible ABA-type triblock copolymers comprising the same PMeOx as the hydrophilic blocks (A) and poly(2-phenyl-2-oxazine), poly(2-phenethyl-2-oxazoline) or poly(2-benzhydryl-2-oxazine), respectively, as the hydrophobic block (B).[41-43] The one with poly(2-phenyl-2-oxazine) allowed for a significantly improved 3D printability and scaffolds stability after blending with alginate. However, the gelation process of this system revealed limitations, such as slow gelation kinetics, which may not be ideal for bioprinting. This problem was overcome when using poly(2-phenethyl-2-oxazoline) as the central hydrophobic block, but these systems need cooling for gelation, which may not be ideal or suitable in all contexts. Therefore, to combine the advantages and offset the drawbacks of the individual components, a novel PMeOx-*b*-PnPrOzi/alginate/clay (POx-*b*-POzi/Alg/clay) hybrid hydrogel bioink was developed in this study, with the clay Laponite XLG as additive for rheological and mechanical improvements during and after printing.

In this advanced POx-*b*-POzi/Alg/clay hybrid hydrogel system, the thermogelling POx-*b*-POzi copolymer ensures good printability and acts as transient physically cross-linked hydrogel that instantly forms post processing also in the presence of Alg, thereby temporarily maintaining the integrity of printed scaffolds. Subsequently, exposure of the printed construct to Ca^{2+} solution initiates the ionotropic crosslinking of Alg to result in an interpenetrating network structure. Distinct from other fugitive ink materials used for fabricating of microvascular/channel networks or hierarchically structured porous hydrogels which are normally printed as bulk separately and removed later on,[44-46] we print a complete structure out of the material directly and then dissolve the fugitive POx-*b*-POzi from the hydrogel blend on the macromolecular level. After dissolution of the temperature sensitive fugitive POx-*b*-POzi network, the ionotropically gelated Alg hydrogel remains and ensures long-term shape stability of the printed constructs. The rheological properties of the hydrogel precursor solutions for printability assessment, mechanical properties of the hydrogels after the ionotropic crosslinking step, as well as the swelling and degradation behavior of the hydrogels were systemically investigated. Accordingly, a variety of three-dimensional constructs, especially the challenging suspended structures were printed successfully with high shape fidelity, stackability and mechanical flexibility, as well as long-term constructs stability. Furthermore, the cell-laden printing and culture with the hydrogels suggests their cytocompatibility and feasibility of the hydrogels as a bioink for 3D bioprinting. We believe that the developed hydrogel in this study will facilitate the potential application of POx-based hydrogels in 3D biofabrication fields, and could be interesting for a wide range of applications including tissue engineering and drug screening.

MATERIALS AND METHODS

Materials. All substances and reagents were obtained from Sigma-Aldrich (Steinheim, Germany) or Acros (Geel, Belgium) and were used as received unless otherwise stated. Reagents used for synthesis of PMeOx-*b*-PnPrOzi (POx-*b*-POzi) diblock copolymer, specifically the initiator methyl trifluoromethylsulfonate (MeOTf),

monomer 2-methyl-2-oxazoline (MeOx), and solvent benzonitrile (PhCN) were dried by refluxing over CaH_2 under dry argon atmosphere followed by subsequent distillation. The monomer 2-*n*-propyl-2-oxazine (nPrOzi), was synthesized by an adapted standard procedure,[47] distilled over CaH_2 and stored under dry argon. Laponite XLG ($[Mg_{5.34}Li_{0.66}Si_8O_{20}(OH)_4]$ $Na_{0.66}$) was purchased from BYK-Chemical GmbH (Wesel, Germany) and used as received. VIVAPHARM® Alginate PH176 (Alg) is extracted from brown algae, approved as a pharmaceutical excipient, and obtained from JRS PHARMA GmbH & Co KG (Rosenberg, Germany). Deionized (DI) water was used throughout the experiments. Murine NIH 3T3 fibroblast (ATTC-Number CRL-1658) were purchased from ATTCC (Manassas, VA, USA). Dulbecco's Modified Eagle Medium (DMEM) was from Sigma-Aldrich (Schnelldorf, Germany), Water-soluble tetrazolium (WST-1) was from Roche (Basel, Switzerland), Fetal bovine serum (FBS) was from Gibco (Darmstadt, Germany) and Penicillin and streptomycin (P/s) solution were purchased from Biochrom AG (Berlin, Germany).

Synthesis and Characterization of POx-*b*-POzi Diblock Copolymer. The POx-*b*-POzi diblock copolymer was synthesized using MeOTf to initiate a cationic ring-opening polymerization of monomers MeOx followed by nPrOzi, as previously described.[36, 39] Specifically, under dry and inert conditions, 0.48 g (2.92 mmol, 1 eq.) MeOTf and 24.81 g (291.5 mmol, 100 eq.) of MeOx were added to 56.58 mL of dry PhCN in a dried flask and polymerized at 120 °C for 4 h. Full monomer conversion was verified by ^{1}H NMR before the addition of the monomer for the second block. After the reaction mixture cooled to ambient temperature, 37.65 g nPrOzi (296.0 mmol, 101 eq.) dissolved in 70.02 mL of dry PhCN was added, kept under continuous stirring at 140 °C overnight. Subsequently, the mixture was cooled again to room temperature, and 1.63 g (8.76 mmol, 3 eq.) of 1-Boc-piperazine was added as terminating agent. The reaction mixture was stirred overnight at 40 °C. After cooling to room temperature, 0.40 g potassium carbonate (2.92 mmol, 1 eq.) was added and the mixture was again stirred for 5 h. Thereafter, the solvent was removed under reduced pressure, the resultant solid polymer mass was dissolved in deionized water, and dialyzed against deionized water using a dialysis membrane with a molecular

weight cut-off (MWCO) of 10 kDa for 2 days. The product was obtained after lyophilization, and named shortly as POx-*b*-POzi (58.3 g, 83.8% yield).

The chemical structure of POx-*b*-POzi was confirmed by ^{1}H NMR on Fourier 300 (300.12 MHz) Bruker BioSpin (Rheinstetten, Germany) at 298 K with $CDCl_3$ as solvent. Gel permeation chromatography (GPC) was performed on an Agilent 1260 Infinity, System Polymer Standards Service (Mainz, Germany) with hexafluoroisopropanol (HFIP) containing 3 g L^{-1} potassium trifluoroacetate (KTFA) as eluent; precolumn: 50 mm × 8 mm PSS PFG linear M; 2 columns: 300 mm × 8 mm PSS PFG linear M (particle size 7 µm; pore size 0.1-1000 kDa). The columns were kept at 40 °C and flow rate was 0.7 mL min^{-1}. Prior to GPC measurement, sample was filtered through a 0.2 µm Teflon filter (Thermo Scientific) to remove particles, if any.

POx-*b*-POzi/Alg/clay Hydrogel Preparation. The POx-*b*-POzi/Alg/clay nanocomposite hydrogel was prepared via thermogelation of the initial blend solutions consisting of POx-*b*-POzi, Alg and clay, followed by ionic crosslinking step. Specifically the preparation of POx-*b*-POzi/Alg/clay hydrogel (20 : 1 : 1.5 wt%) was performed as follows. Initially, 0.015 g clay and 0.01 g Alg were dispersed in 0.775 g DI water with continuous stirring for few minutes. Subsequently, 0.2 g lyophilized POx-*b*-POzi copolymer was added into the mixture, and then stored at 7 °C (for at least 24 h) to allow complete polymer dissolution and to obtain a homogeneous dispersion. The dispersion was then transferred to a defined mould in cold state, and kept at room temperature for ten minutes to trigger the thermogelation process of POx-*b*-POzi/Alg/clay solution. Successively, the mould was immersed into 1 wt% $CaCl_2$ aqueous solution overnight to complete the further curing step of ionic crosslinking with Ca^{2+}. The final POx-*b*-POzi/Alg/clay hydrogels were obtained followed by washing twice with DI water. For comparison, different POx-*b*-POzi/Alg hydrogels without clay were also prepared. In addition, the ionic crosslinking diversity of the hydrogels was also confirmed by replacing the $CaCl_2$ solution for ionic crosslinking step with $FeCl_3 \cdot 6H_2O$ (0.3 mol L^{-1}) or $TbCl_3 \cdot 6H_2O$ (0.3 mol L^{-1}) solution.

Hydrogel Characterizations.

Solid content. Solid content (Gel content) of the hydrogels was calculated using formula M_1/M_0 (n=3), where M_0 and M_1 are the weight of the swollen hydrogels and the corresponding weight of lyophilized swollen hydrogels after incubation for regular intervals in DI water at room temperature, respectively. The DI water was replaced every day.

Swelling ratio (SR). The SR of the hydrogel was assessed using a gravimetric method. Initially, the dry weight (W_d) of hydrogels was noted, followed by immersion in DI water at room temperature. At predefined time points, the wet hydrogels were taken, the excess surface liquid was cleared using blotting paper, and the swelled weight (W_t) was recorded. The study was conducted under identical conditions in triplicates, and the SR was calculated using the equation $SR = (W_t - W_d)/W_d$.

Scanning electron microscopy (SEM). The hydrogels were frozen with liquid nitrogen and lyophilized afterwards. The dried hydrogel samples were mounted on aluminum sample holders with conductive carbon tape and sputtered with platinum in a sputter coater Leica Microsystems ACE 400 (Wetzlar, Germany). The morphology of the samples was subsequently analyzed using a Crossbeam 340 field emission scanning electron microscope Carl Zeiss Microscopy (Oberkochen, Germany) by setting the acceleration voltage ETH to 2.0 kV.

Rheological Property Measurements. Rheological measurements were performed using the MCR 301 rheometer from Anton Paar (Ostfildern, Germany) employing a 25 mm diameter parallel-plate geometry. A Peltier system was employed for temperature control. Under a constant angular frequency and strain of 10 rad s^{-1} and 0.5% respectively, the temperature sweeps from 5 to 45 °C were carried out at a heating rate of 0.05 °C s^{-1} to study the thermogelling behavior. Then, amplitude sweeps in the oscillation strain range of 0.01-500% was performed at a constant angular frequency of 10 rad s^{-1}, from which the linear viscoelastic (LVE) range was determined. The frequency sweep was performed in an angular frequency range of 0.1-100 rad s^{-1} at a certain strain of 0.1% (within the LVE range obtained from the amplitude sweep). To evaluate the yield stress/yield point of a hydrogel system,

dynamic oscillatory stress sweep and steady stress sweep were performed. In dynamic oscillatory stress sweep, yield stress was evaluated using onset determination, and the flow point is determined as the crossing of storage and loss modulus (G' = G'') by definition. In steady stress sweep, the corresponding shear stress where the viscosity starts decreasing by several orders of magnitude is referred to as yield stress. What's more, steady-state shear flow from 0.01 to 1000 s^{-1} of shear rate were performed to characterize the shear thinning behavior. The obtained viscosity η decrease was fitted using the power-law expression $\eta = K\cdot(\dot{\gamma})^{n-1}$ established by Ostwald−de Waele, where K is the consistency index, n is the flow index, and $\dot{\gamma}$ is the applied shear rate. Finally, to investigate recovery properties, time sweeps of shear flow with alternating shear rate of 0.1 s^{-1} and 100 s^{-1} were performed. Except for the temperature sweep, all tests were performed at 37 °C. An aqueous solvent trap was utilized in all experiments to mitigate drying effects.

Mechanical Compression Tests. Mechanical compression was tested by universal testing machine Zwick Roell Z010 (Ulm, Germany) with a force sensor of 100 N at room temperature. Cylindrical hydrogel discs (10 mm diameter, 6 mm height) were prepared and tested at a constant compression speed of 1 mm min^{-1}. Young's modulus was determined in the 0–20% initial linear strain region. Each measurement was performed in triplicate and results are reported as the mean ± standard deviation.

3D Printing. An extrusion-based 3D bioprinter CELLINK BIO X (Gothenburg, Sweden) was used for 3D printing of hydrogel constructs. The prepared hydrogel precursor solution was loaded as the ink material into a printing cartridge in liquid (cooled) form conveniently because of its thermogelling property, and then kept in 7 °C fridge to eliminate bubbles before printing. For printing, the ink loaded pneumatic syringe dispenser was equipped with a 0.33 mm inner diameter precision needle (23G), and then driven pneumatically through the nozzle to extrude the hydrogel onto the preheated 37 °C print-bed in a layer-by-layer deposition mode. The printing speed was fixed at 4 mm s^{-1} in all printing experiments. The extrusion pressure was controlled and varied from 70 to 110 kPa according to different

user-defined printing structures which are programmed by G-code. Immediately after printing, the printed structures were physically cured by immersing into $CaCl_2$ (or $FeCl_3 \cdot 6H_2O$, $TbCl_3 \cdot 6H_2O$) aqueous solution to complete the Alg crosslinking followed by washing twice with DI water.

Cell culture and cytocompatibility of bioink. The murine-derived NIH 3T3 fibroblast were maintained under standard culture conditions (37 °C and 5% CO_2) in DMEM supplemented with 10% FBS and 1% P/s. The WST-1 assay was performed to evaluate the compatibility of bioink via treatment of different concentration of bioink in growth media and encapsulation of cells in bioink. Briefly, 1 x 10^5 fibroblasts were cultured overnight in 96 well plate. Next day, POx-*b*-POzi (20 wt%), POx-*b*-POzi/Alg (20 : 1 wt%), and POx-*b*-POzi/Alg/clay (20 : 1 : 1.5 wt%) hydrogel precursor solutions (ink materials) prepared in filtered-sterile DI water were further sterilized under UV light for 1h and diluted into 10, 5, 1.5, and 1 wt% in ice-cold fresh growth media. About 100 µL of each diluted polymer in growth media was added to their assigned cell groups (n=4) and incubated for 24 h under standard culture conditions. Thereafter, treated media was carefully removed and cells were washed with PBS. Subsequently, cells were treated with freshly prepared WST-1 reagent solution for 1 h according to manufacturer's instruction and absorbance values were recorded at 450 nm using Spark 20M multimode microplate reader (Tecan, Germany). Further, fibroblasts, with density of 1 x 10^6 cell per mL, were incorporated into hydrogel precursor solutions (POx-*b*-POzi (20 wt%), POx-*b*-POzi/Alg (20 : 1 wt%), and POx-*b*-POzi/Alg/clay (20 : 1 : 1.5 wt%)) and were thoroughly mixed on ice bath. Then, 100 µL of cell-laden hydrogel solutions were added into specified wells of each group (n=4) in pre-warmed 96 well plate. While POx-*b*-POzi/Alg and POx-*b*-POzi/Alg/clay groups were followed by ionic crosslinking for 10 min with 1 wt% $CaCl_2$ aqueous solution filtered through a sterile 0.2 µm membrane. Thereafter, $CaCl_2$ solution was removed and crosslinked hydrogels were washed thrice in PBS. About 100 µL of fresh media was added into each well and cell-laden hydrogels were incubated under standard culture conditions. Finally, WST-1 assay was performed at day 1 and day 3 as described before.

Cells proliferation and viability in 3D bioprinted constructs. To investigate the proliferation and viability of cells in bioprinted construct, fibroblast (1 x 10^6 cells per mL) were incorporated into POx-*b*-POzi/Alg (20 : 1 wt%) and POx-*b*-POzi/Alg/clay (20 : 1 : 1.5 wt%) hydrogel precursor solutions (ink materials) as discussed earlier. Thereafter, the bioinks were transferred into the pneumatic syringe dispenser equipped with the needle of 23 G, and then printed as the previously described. Subsequently, bioprinted constructs were treated with pre-sterile $CaCl_2$ solution (1 wt%) for 10 min for ionic crosslinking following 3-time washing in PBS. About 3 mL of growth media was added into each sample and media was changed on every alternative day and cell distribution in bioprinted constructs was analyzed at day 1 and day 5 using optical microscope. The DNA assay was performed to assess the proliferation of cells in each group (n=6) at day 1, 3, and 5. Briefly, samples were collected on each interval of times, washed thrice in PBS, and treated with 300 µL of RIPA buffers (150 mm Trizma-base, 150 nm NaCl, 1% sodium deoxycholate, 0.1% SDS, and 1% Triton X ‑ 100 in distilled water). The samples were chopped in RIPA buffers and supernatants were collected after centrifugation at 12.000 rpm for 10 min. Then, DNA assay was performed using with Quant-iT PicoGreen dsDNA assay kits (Invitrogen, Carlsbad, CA, USA) according to the manufacturer's guidelines. The Live and Dead assay was performed to visualize the viability of cells in POx-*b*-POzi/Alg/clay bioprinted construct at day 1 and day 5. Briefly, bioprinted constructs were incubated a working solution of ethidium homodimer (1:500) and calcein-AM (1:1000) prepared in DPBS for 30 min. Finally, images of live and dead cells were acquired through a fluorescent microscope (Zeiss Axioimager Z1 microscope).

RESULTS AND DISCUSSION

Polymer Synthesis and Characterization. The diblock copolymer PMeOx-*b*-PnPrOzi was synthesized by LCROP of the monomers MeOx and nPrOzi as previously reported and characterized accordingly (Figure S1, Supporting Information).[36, 39] From the signals in the ^{1}H NMR spectrum with chemical shifts at 2.10 ppm (CH_3 of PMeOx) and

0.94 ppm (CH_3 of PnPrOzi), the relative block lengths and diblock copolymer composition was determined to be $PMeOx_{110}$-*b*-$PnPrOzi_{112}$ (hereafter noted as POx-*b*-POzi) with a number-average molar mass (M_n) of around 24 kg mol^{-1} *via* end group analysis. A dispersity of Đ = 1.3 obtained from GPC analysis indicating that the diblock copolymer was obtained with reasonable control and definition.

POx-*b*-POzi/Alg/clay Hydrogel Preparation. In preliminary experiments, hydrogels with different compositions were prepared and analyzed with respect to their thermogelling behavior (Table S1 and Figures S2a, Supporting Information). Specifically, 20 wt% POx-*b*-POzi were combined with 1, 2 and 3 wt% sodium alginate. Also, a ternary mixture of 20 wt% POx-*b*-POzi, 1 wt% sodium alginate and 1.5 wt% clay was prepared. This screening showed that higher weight concentrations of Alg make the precursor mixture solution highly viscous, increased the loss factor tan δ (G''/G'), and weakened thermogelling property. Therefore, we chose to only investigate 1 wt% sodium alginate in more detail. Unless otherwise noted, the precursor mixtures of POx-*b*-POzi/Alg/clay (POx-*b*-POzi/Alg/ clay = 20/1/1.5; w/w) and POx-*b*-POzi/Alg (POx-*b*-POzi/ Alg = 20/ 1; w/w) were investigated in this study. Specifically, the POx-*b*-POzi/Alg/clay hydrogel was prepared using a simple two-step approach (Figure 1a). In the first step, the dry components (POx-*b*-POzi, Alg and clay) were mixed in the desired ratios and dissolved at 7 °C in DI water to obtain a homogeneous solution. Subsequently, when the mixture is allowed to warm to room temperature for few minutes, thermogelation will take place. It should be noted that the thermogelation is completely reversible upon cooling (Figure 1b, Video S1 in Supporting Information). In the second step, the hydrogel was immersed at room temperature in a 1 wt% (0.09 M) $CaCl_2$ solution overnight, to allow the ionotropic crosslinking of Alg, resulting in a stable and mechanical flexible POx-*b*-POzi/Alg/clay hydrogel. During this process, Ca^{2+} ions diffused into the hydrogel network and crosslinked the sodium alginate through coordination with $-COO^-$ groups. Concomitantly, the POx-*b*-POzi diblock copolymer can gradually diffuse out of the hydrogel network and dissolve, especially in the first 2 h, as demonstrated by a step decrease in the gel content (Figure S2b, Supporting Information).

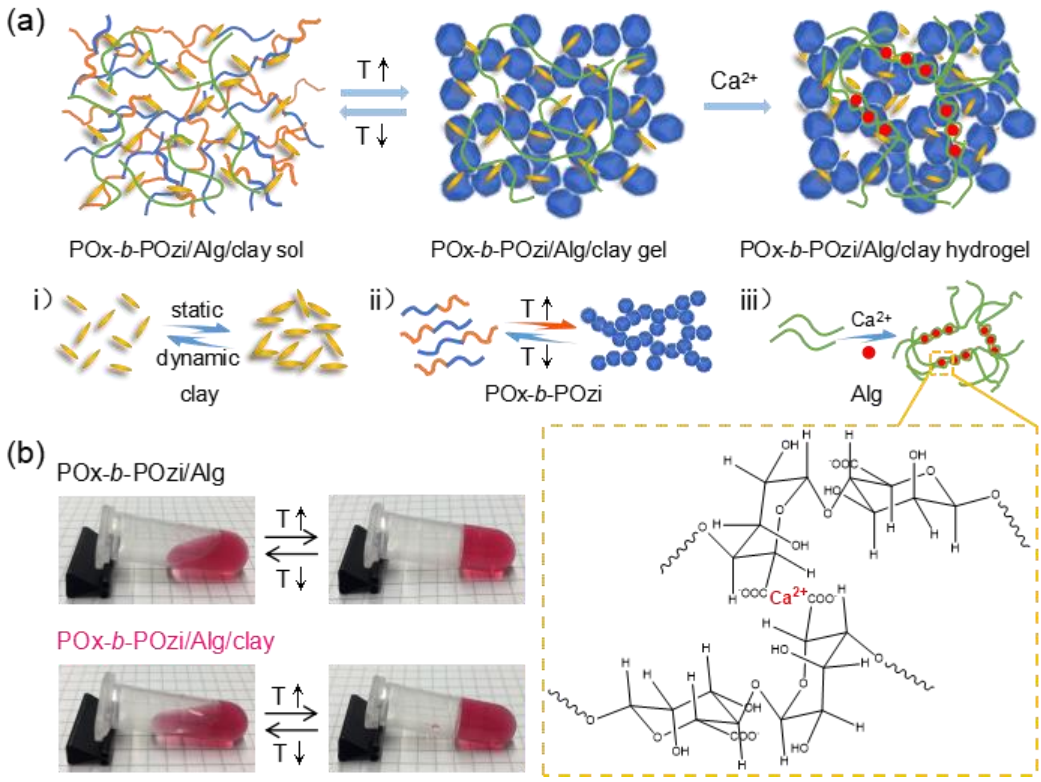

Figure 1. (a) Schematic illustration for the preparation of POx-*b*-POzi/Alg/clay hydrogel *via* the strategy of thermogelation and subsequent ionic crosslinking of Alg with Ca^{2+}. (b) Photographs demonstrating the thermo-reversible sol-gel transition of POx-*b*-POzi/Alg and POx-*b*-POzi/Alg/clay hydrogel precursor solutions before ionic crosslinking (dyed by carmine).

Subsequently, the long-term stability of the hydrogels in DI water was assessed over a one-month period by measuring the solid/gel content over time (Figure 2a). Both POx-*b*-POzi/Alg and POx-*b*-POzi/Alg/clay hydrogel underwent a decrease of gel content, especially in the first day, and reached a plateau after 7 d. Finally, solid contents of around 6.6 wt% for POx-*b*-POzi/Alg hydrogel and 4.1 wt% for POx-*b*-POzi/Alg/clay hydrogel were obtained. At this point, we assume that predominantly the POx-*b*-POzi diblock copolymer is leached from the hydrogel networks while the ionically crosslinked alginate and clay nanoparticles remain behind. However, some diblock copolymer must remain trapped in the alginate hydrogel to explain the final solid content. Important to note, the shape and volume of the hydrogels did not undergo any visible change, which is very favorable as this avoids the need for complex calculations for swelling or shrinkage of 3D printed constructs (the insert photographs in Figure 2a).

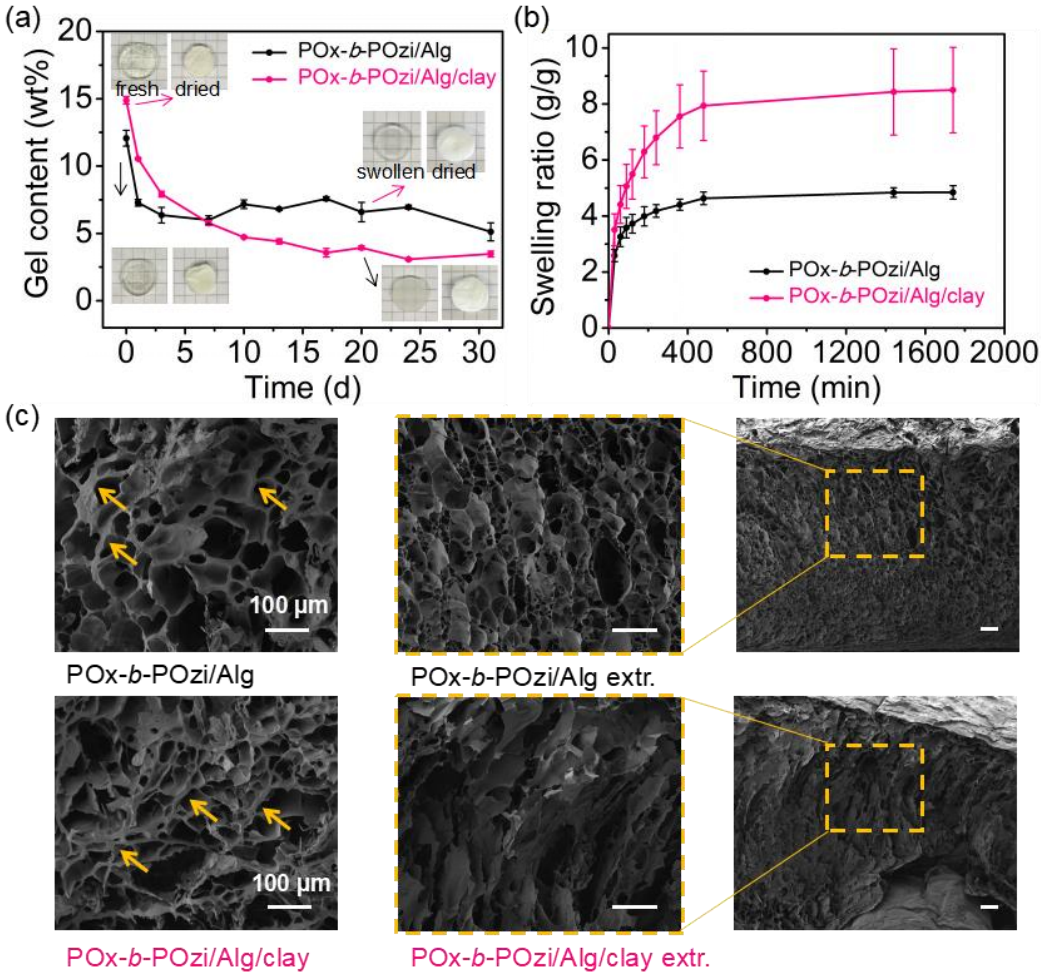

Figure 2. (a) Determination of gel content of the hydrogels after Ca^{2+} crosslinking in DI water at 37 °C. Insert photographs represented the corresponding hydrogel appearance at different stages, the background is 5 × 5 mm grid. (b) Swelling behavior of the hydrogels in water at room temperature. (c) SEM images of the hydrogels before and after thoroughly washing (the yellow arrow added as a guide for the eye to thick patches of hydrogel pore walls). Scale bar: 100 µm.

Furthermore, the dried (lyophilized) materials were also studied with respect to their swelling kinetics in DI water until equilibrium was reached (Figure 2b). Both hydrogels presented a fast swelling rate in an initial stage, and then plateaued off at an equilibrium swelling ratio of 480% for the POx-*b*-POzi/Alg hydrogel, and 840% for the POx-*b*-POzi/Alg/clay hydrogel, which may be due to the presence of highly hydrophilic clay Laponite XLG. SEM images of the hydrogels after 7 days extraction (POx-*b*-POzi/Alg extr. and POx-*b*-POzi/Alg/clay extr.) suggest that the hydrogel networks become more uniform with thinner pore walls in comparison to the freshly prepared samples (yellow arrows in Figure 2c). Interestingly, for POx-*b*-POzi/Alg/clay hydrogel, it appears that the typical layered house-of-cards structure of clay can be

observed after 7 days of thorough washing/extraction.[48] As the majority of POx-*b*-POzi diblock copolymer is extracted, the remaining clay appears to dominant hydrogel network morphology, presumably both alginate and remaining POx bind to the clay nanoplatelets via electrostatic and H-bonding interaction, respectively (Figure 2c).

Rheological Properties of POx-*b*-POzi/Alg/clay Hydrogel Precursor Solution. Rheological measurements were carried out to understand the viscoelastic behavior and estimate the printability of the hydrogel precursor solutions.[49-50] Initially, the thermogelling behavior was investigated using a dynamic oscillation temperature sweep, wherein the intersection of storage modulus (G') and loss modulus (G") defines the gel point, and the corresponding temperature as the gel temperature (T_{gel}) (Figure 3a). Both POx-*b*-POzi/Alg/clay and POx-*b*-POzi/Alg mixtures maintained and exhibited typical thermogelling behavior of the pristine POx-*b*-POzi hydrogel (T_{gel} ≈ 17 °C and G'_{max} ≈ 3.3 kPa).[36, 39] POx-*b*-POzi/Alg and POx-*b*-POzi/Alg/clay exhibited a comparable thermogelling behavior with slightly increased moduli (G', G") with a G'_{max} ≈ 4.5 kPa. Addition of Alg lead to minor increase in T_{gel} (19 °C). In contrast, when also clay was added, a small decrease in T_{gel} (15 °C) was observed. Such remarkable thermoresponsive transition between liquid-like and solid-like of the mixtures will not only facilitate the effective mixing of the hydrogel ink with cells and other substances, but also avoid undesired cells aggregation and settlement at the same time, and is generally highly beneficial for sample handling. An amplitude sweep was conducted to assess the LVE range, which appears as the onset of the decrease of G' (and increase in G'') and indicates the beginning of the collapse of the hydrogel's inner structure (Figure 3b). The clay addition leads to an extension of the LVE, which is in line with observations for the plain POx-*b*-POzi thermogelling system.[39] A subsequent dynamic frequency sweep under a strain of 0.1% within the LVE range showed a dominating G' value over G'' in the entire investigated frequency range (0.1-100 rad s^{-1}), indicating their stable gel-like character (Figure 3c). While the G' were rather stable, the values for G'' went through a minimum at around 10 rad s^{-1}.

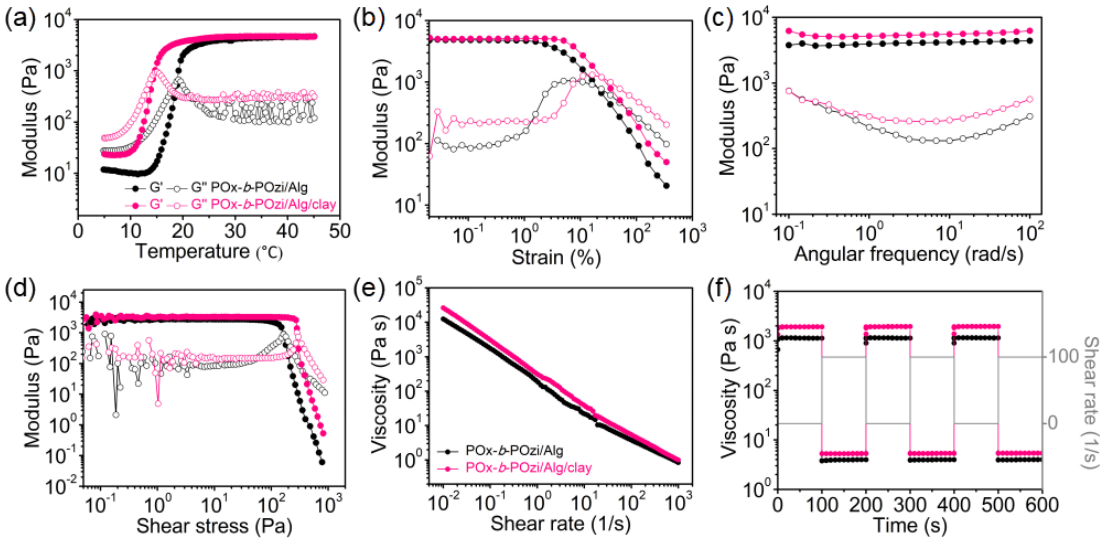

Figure 3. Rheological characterization of the POx-*b*-POzi/Alg and POx-*b*-POzi/Alg/clay hydrogel precursor solutions. (a) A plot of the temperature sweep from 5 to 45 °C. (b) Amplitude sweep at an angular frequency of 10 rad/s to determine the LVE range. (c) Frequency sweep at an applied strain of 0.1%. (d) Development of storage (G') and loss (G") modulus with increasing shear stresses. (e) Shear thinning behavior. (f) Recovery property under alternative applied shear rate of 0.1 s^{-1} and 100 s^{-1}.

The yield stress is a critical parameter for printability. It defines the hydrogel´s resistance against deformation from gravity or surface tension, and therefore, is a potential predictor of how well an ink keeps its shape fidelity after extrusion.[49-50] From the dynamic oscillatory stress sweep, a well improved yield stress of around 210 Pa was observed for POx-*b*-POzi/Alg/clay mixture, compared to only 80 Pa for POx-*b*-POzi/Alg mixture (Figure 3d). Such yield stress improvement was corroborated in a rotational steady stress sweep, which yielded 180 Pa for POx-*b*-POzi/Alg/clay and 90 Pa for POx-*b*-POzi/Alg (Figure S3, Supporting Information). The yield stress of plain POx-*b*-POzi hydrogel was 140 Pa, as determined in a steady stress sweep, while addition of clay increased the yield stress to 240 Pa.[39] Therefore, it appears that the addition of 1 wt% alginate generally decreases the yield stress of the POx-*b*-POzi thermogel while addition of clay increases it and overcompensates the loss from alginate addition. Furthermore, another parameter important for 3D printing is the shear-thinning of the material. Here, the viscosity of the different mixtures decreased rather markedly over five orders of magnitude along with the increasing shear rate from 0.01 to 1000 s^{-1}, indicating their pronounced shear-thinning behavior (Figure

3e). By fitting the shear rate-viscosity rheology profile using a power-law expression, the flow index n and the consistency index K were obtained. Not surprisingly, the clay addition lead to an enhanced shear-thinning character (POx-*b*-POzi/Alg/clay; n = 0.07 and K = 368.4 vs POx-*b*-POzi/Alg; n = 0.14 and K = 246.5). Important to note, the addition of alginate does lead to a slightly increased viscosity of the mixtures, irrespective of temperature and shear, which is relevant for e.g., dispersing cells into the hydrogel.

Finally, very rapid structure recovery was observed for both mixtures (Figure 3f). Such almost instantaneously viscosity recovery after changing from high (100 s^{-1}) to low (0.1 s^{-1}) shear rates is highly desirable for materials used for extrusion-based 3D bioprinting. This, together with the shear-thinning character, can facilitate an efficient dispensing of the bioink through fine nozzles without affecting the cell viability, and subsequently retain the shape of the printed objects with high-resolution and high-fidelity. In summary, the rheological measurements revealed that both POx-*b*-POzi/Alg and POx-*b*-POzi/Alg/clay systems exhibited thermogelling property with pronounced shear thinning character and rapid viscosity recovery property, suggesting their great potential as ink material for 3D bioprinting. However, in comparison, POx-*b*-POzi/Alg/clay might be considered a better bioink candidate, not only because of the reported bioactivity of clay in biological study,[51-53] but also due to the comprehensively improved rheological properties from clay addition, in specific the shear thinning character, yield stress and viscosity, which are all crucial parameters for high printing performance prediction. The fast thermogelation, shear-thinning and structure recovery of the mixtures is excellently suited to temporarily maintain the printed shapes. However, any additional mechanical stress after printing or addition of excess water/aqueous media would destroy or dissolve any printed structure easily. To prevent this, the influence of the ionically crosslinked alginate component in the present composite material is studied in this study.

Mechanical Properties of POx-*b*-POzi/Alg/clay Hydrogel. After Ca^{2+} curing, the mechanical properties of the hydrogel were evaluated by frequency sweep and compression tests. Initially, dependence of average G' on angular frequency (25 mm diameter × 5 mm height) after different Ca^{2+} crosslinking times was investigated (Figure 4a, Figure S4 in Supporting Information). During the incubation with $CaCl_2$ solution, Ca^{2+} ions gradually diffuse into the hydrogel network and crosslinked the Alg, resulting in a stiffening of the hydrogel, as reflected in the continuous increasing of G'. In both POx-*b*-POzi/Alg and POx-*b*-POzi/Alg/clay hydrogels, the G' plateau at about 4 h, and reached the maximum G' of 32.4 ± 3.3 kPa and 29.2 ± 2.6 kPa, respectively, corresponding to a more than 6-fold increase over the non-crosslinked samples. Of course, the required crosslinking time will increase when the thickness of sample increases, and vice versa. After 23 h soaking in $CaCl_2$ solution, we observed a minor decrease of G', which may be attributed to a continuous extraction and elution of POx-*b*-POzi diblock copolymer from the hydrogels (Figure S2b, Supporting Information).

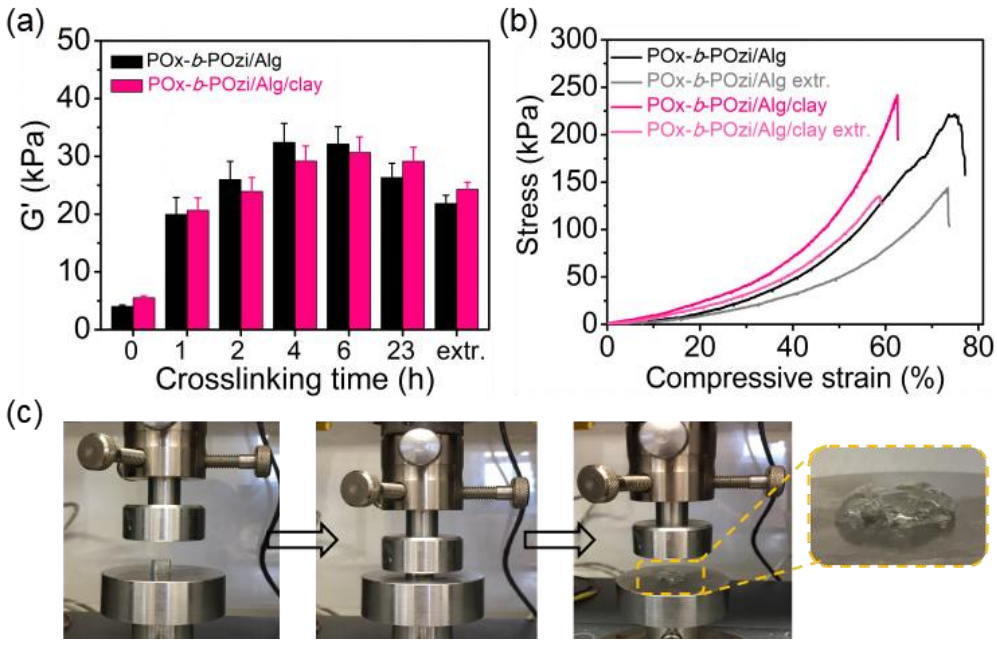

Figure 4. (a) Development of storage moduli (G') of POx-*b*-POzi/Alg and POx-*b*-POzi/Alg/clay hydrogels over time after addition of Ca^{2+} as a crosslinker. Storage moduli after extensive washing/extraction are shown for comparison. (b) Stress-strain curve under compression for various hydrogel samples before and after extensive washing/extraction. (c) Photographs during the compression test of POx-*b*-POzi/Alg hydrogel.

Table 1: Compression testing of the hydrogels.[#] hydrogels	Young's modulus (kPa)	strength (kPa)	breaking strain (%)
POx-*b*-POzi/Alg	35.0 ± 0.6	204 ± 14	72.2 ± 4.3
POx-*b*-POzi/Alg extr.[#]	30.5 ± 0.9	139.4 ± 2.8	72.4 ± 0.8
POx-*b*-POzi/Alg/clay	94.6 ± 5.9	238 ± 13	61.9 ± 1.1
POx-*b*-POzi/Alg/clay extr.[#]	65.5 ± 9.1	131.3 ± 3.8	57.8 ± 2.5

[#] The compression testing of hydrogels was carried out after immersion in DI water for 7 d. The DI water was exchanged daily.

In fact, after 7 days of exhaustive extraction, the hydrogels reached a swelling equilibrium whereby the values for G' decreased slightly to 21.8 ± 1.4 kPa for POx-*b*-POzi/Alg and 24.3 ± 1.2 kPa for POx-*b*-POzi/Alg/clay. No significant differences between G' values between Ca^{2+} crosslinked hydrogels were found. Subsequently, compression tests were carried out on the hydrogels after Ca^{2+} crosslinking (Figure 4b-c, Table 1). The compressive stress at break for POx-*b*-POzi/Alg/clay hydrogel (238 ± 13 kPa) was slightly higher but comparable to POx-*b*-POzi/Alg hydrogel (204 ± 14 kPa). In contrast, the compressive Young's modulus of POx-*b*-POzi/Alg/clay hydrogel (94.6 ± 9.1 kPa) was significantly improved due to the incorporation of clay, and found around 3 times higher than the value for POx-*b*-POzi/Alg hydrogel (35.0 ± 0.6 kPa). After allowing the hydrogels swell to equilibrium in DI water, both compressive strength and Young's modulus decreased to 131.3 ± 3.8 kPa and 65.5 ± 9.1 kPa for POx-*b*-POzi/Alg/clay, and 139.4 ± 2.8 kPa and 30.5 ± 0.9 kPa for POx-*b*-POzi/Alg, respectively. Interestingly, the decrease in compressive Young's modulus was somewhat more pronounced in case of POx-*b*-POzi/Alg compared to POx-*b*-POzi/Alg/clay, which may be attributed to the higher swelling degree of the latter. Additionally, there was no significant difference in the breaking strain before and after exhaustive extraction (Table 1).

3D Printing. The hydrogels inks were processed by an extrusion-based 3D printer to investigate their 3D printability (Figure S5a, Supporting Information). Initially, a 12-layer hollow five-pointed star (7.28 × 7.28 mm) and a 12-layer 5 x 5 line grid (20 × 20 mm) were printed using POx-*b*-POzi/Alg hydrogel under an extrusion pressure of

80 kPa. Thereafter, the constructs were crosslinked by immersion in a $CaCl_2$ solution for 6h. The final scaffolds proved to be mechanically flexible and rather robust with respect to manual handling and compression (Figure 5a-b). The highly shear-thinning character of the POx-*b*-POzi/Alg mixture allows extrusion of smooth filaments through the fine needle (23 G). At the same time, the hydrogel properties allow printing at room temperature or, as performed here, at physiological temperature on a heated (37 °C) print bed. More importantly, the 3D structures remained geometrical stable without obvious collapse and volumetric swelling after 7 days incubation in DI water (Figure 5b). Alternatively, the printed structures can also be cured using other multivalent cations, as demonstrated by Fe^{3+} and Tb^{3+}, by simply exchanging the $CaCl_2$ (aq.) to $FeCl_3{\cdot}6H_2O$ or $TbCl_3{\cdot}6H_2O$ (aq.). Consequently, the Fe^{3+} crosslinked printed structures appeared as yellow and the Tb^{3+} crosslinked printed structures were photoluminescent (Figure 5c-d).

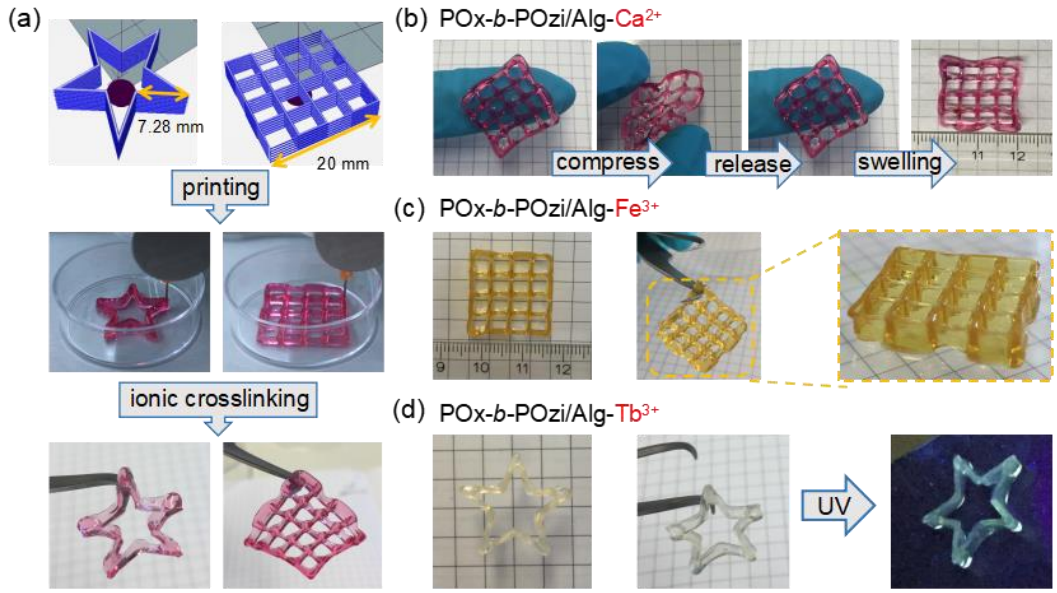

Figure 5. Extrusion-based 3D printing of POx-*b*-POzi/Alg hydrogel ink. (a-b) Illustration of the CAD models of a 12-layer five-point star and a 12-layer 5 x 5 line grid and the 3D printing process. After printing, the structures were cured by immersion into a $CaCl_2$ solution by which removed the fugitive support ink concomitantly. The obtained structures were mechanical flexible under compressing, and remained stable after equilibrium swelling. Hydrogels dyed using carmine. As crosslinkers, also $FeCl_3{\cdot}6H_2O$ (c) and $TbCl_3{\cdot}6H_2O$ (d) were employed. Crosslinking using $TbCl_3{\cdot}6H_2O$ imparts photoluminescent (excitation under UV light) properties in the scaffolds. The photo background is 5 × 5 mm grid.

Although we did not investigate this aspect in any detail, it should be clear that different crosslinking ions should also allow for tuning the mechanical properties.The successful printing of designed 3D constructs with high shape fidelity demonstrated that POx-*b*-POzi/Alg hydrogel are a suitable ink material for extrusion-based 3D printing technology. Subsequently, the printing performance of three different hydrogel inks (POx-*b*-POzi, POx-*b*-POzi/Alg and POx-*b*-POzi/Alg/clay) were investigated in more detail.[54] Firstly, a serrated mold with a stepwise increasing gap from 1, 2, 4, 8 to 16 mm was used for filament collapse test under a constant extrusion pressure of 110 kPa (Figure 6a, Video S2 in Supporting Information). When using POx-*b*-POzi/Alg/clay, the printed strand could hang on the mold relatively stably (for several minutes) even for a gap of up to 16 mm. The filament did sag significantly and after extended time will eventually give in to gravity. In contrast, the POx-*b*-POzi and POx-*b*-POzi/Alg hydrogel were much weaker and broken off immediately at a smaller gap of only 4 and 8 mm, respectively. In the filament fusion test, 2D patterns with stepwise increasing strand distances varying from 0.5 to 0.75, 1, 1.25 and 1.5 mm were printed for assessment of filament fusion and the minimal strand-to-strand distance (Figure 6b). Obviously, this test is also highly dependent on printing parameters such as nozzle size, printing speed and extrusion pressure. Here, all these experiments were carried out with a 23G needle (inner diameter of 0.33 mm) at a fixed printing speed of 4 mm s^{-1} and an extrusion pressure of 70 kPa. Again, printability in the order of POx-*b*-POzi/Alg/clay > POx-*b*-POzi/Alg > POx-*b*-POzi was observed. For POx-*b*-POzi and POx-*b*-POzi/Alg, filament fusion was observed at strand-to-strand distances below 1.25 and 1 mm, respectively. Using POx-*b*-POzi/Alg/clay, the same grid was printed without notable strand fusion or collapse. The printed strands remained excellently defined even at strand-to-strand distances below 0.75 mm. Again, the rheological benefit of the addition of clay is clear and can be attributed specifically to the improved viscosity and yield stress in combination with an increased shear-thinning character resulting in this significant improvement in the stackability and shape fidelity during printing process.

Accordingly, we extended the height of printed 3D structures to a 24-layer 5 x 5 line grid and a hollow 20-layer five-point star (Figure 6c), and even a 60-layer hollow cube successfully (Figure S5b, Supporting Information). Even such high construct did not buckle noticeably under their own weight. The intersections of the grid and sharp corners of the star were excellently resolved. Again, after curing by Ca^{2+}, mechanically flexible hydrogel scaffolds were obtained, which can be readily manipulated using tweezers.

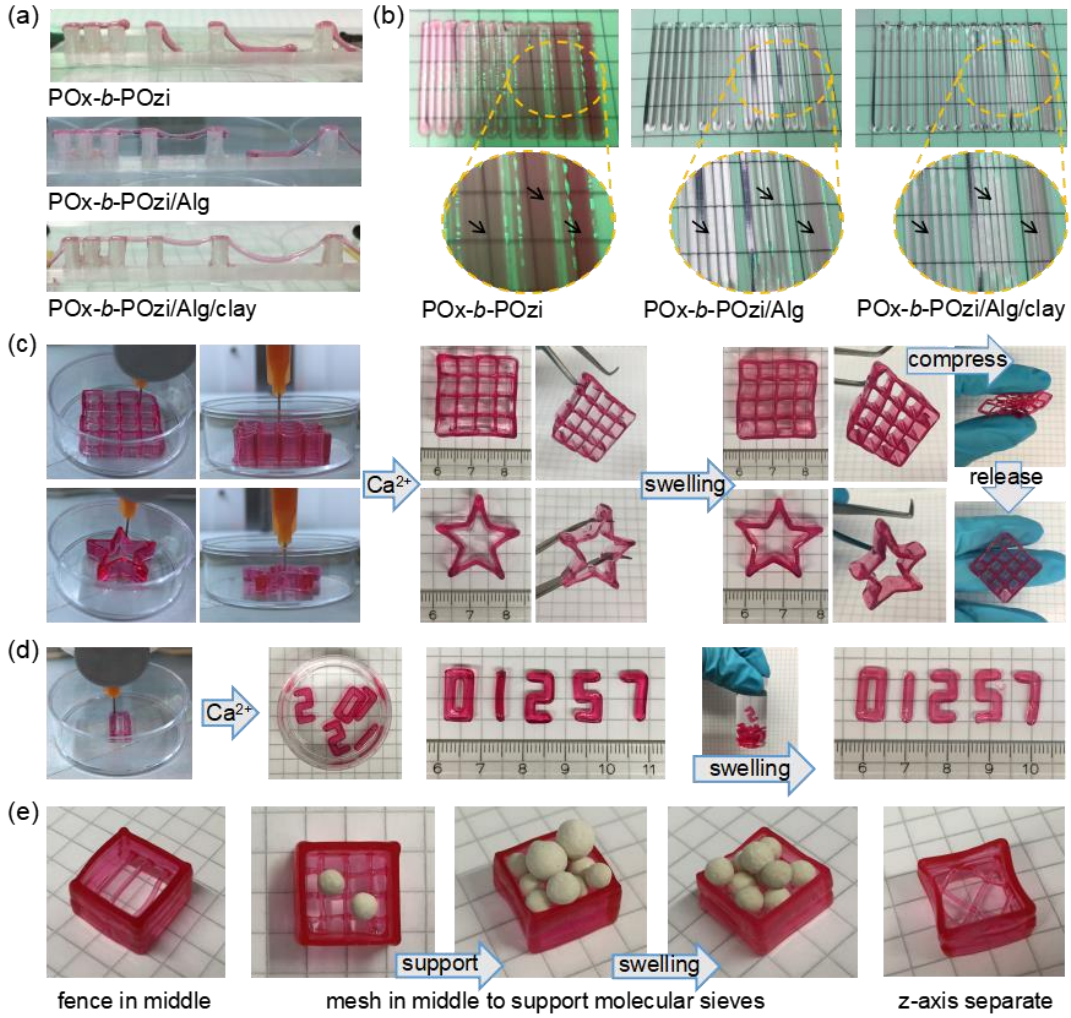

Figure 6. (a) Filament collapse test of various hydrogel inks with a stepwise increase in gap from 1, 2, 4, 8 to 16 mm. Addition of alginate and clay both improve filament stability. (b) Filament fusion test of various hydrogel inks with a stepwise increase in strand-to-strand distance from 0.5, 0.75, 1.0, 1.25 to 1.5 mm. (c) 3D printing and ionic crosslinking of a 24-layer 5 x 5 line grid and a 20-layer five-point star with POx-*b*-POzi/Alg/clay hydrogel ink. (d) 3D printing of 4-layer numeral with POx-*b*-POzi/Alg/clay hydrogel ink. (e) 3D printing of different 20-layer constructs line-grids with suspended filaments able to hold molecular sieves granules. The extrusion pressure is 110 kPa in figure 6c-e. Scaffolds dyed using carmine. The photo background is 5 × 5 mm grid.

Just as with printed hydrogel without clay, the constructs containing clay were stable after 7 days incubation in DI water, and still exhibited remarkable mechanical flexibility upon compression deformation. For demonstration purposes, several 4-layer Arabic numerals were also printed. Finally, very challenging constructs containing filaments suspended over 10 mm were also printed successfully with high shape fidelity, without the need of any additional sacrificial support material. This demonstrates the extraordinary printability design freedom possible when using POx-*b*-POzi/Alg/clay hydrogel (Figure 6d-e, Video S3 in Supporting Information).

Cytocompatibility and 3D Cell-laden Printing. In order to be considered as a suitable bioink, the novel hybrid materials must be cytocompatible. Using the WST-1 assay, no significant reduction in metabolic activity of NIH 3T3 cells were observed when incubated with 1, 1.5, 5, and 10 wt% solutions of POx-*b*-POzi, POx-*b*-POzi/Alg, and POx-*b*-POzi/Alg/clay in growth media over 24 h (Figure S6a, Supporting Information). In fact, cell-laden hydrogel revealed a significant increase in cell number from day 1 to day 3. Optical microscopy analysis revealed a throughout homogenous distribution of cells in POx-*b*-POzi/Alg and POx-*b*-POzi/Alg/clay groups with distinct increase in cell number on day 3 (Figure S6b, Supporting Information). In contrast, cells in POx-*b*-POzi hydrogel started aggregation at day 1 and formed relatively large aggregates at day 3. This observation can be attributed to the gradual dissolution of POx-*b*-POzi in media to form a viscous solution, which facilitated cell aggregation, settlement and attachment of aggregates at bottom of the well plates. Therefore, we excluded plain POx-*b*-POzi from further studies. Corroborating the impression from optical microscopy, WST-1 assay showed a significant increase in metabolic activity at day 3 in POx-*b*-POzi/Alg and POx-*b*-POzi/Alg/clay indicating proliferation of fibroblasts in hydrogels with no significant difference between the groups (Figure S6c, Supporting Information).

Further, we analyzed the distribution, proliferation, and viability of fibroblasts in 3D bioprinted construct. Important to note cells were homogenously distributed in 3D bioprinted construct (5 x 5 line grid, 8-layer; 12 $\times$ 12 mm) of POx-*b*-POzi/Alg and POx-*b*-POzi/Alg/clay (Figure 7a). The ionically crosslinked constructs printed using

both bioinks showed a good structural stability over 5 days of cell culture. Corroborating results from cell-free printing, the POx-*b*-POzi/Alg/clay bioink exhibited a better printability. We should point out that the presence of cells and cell culture media was not detrimental to the 3D printability, which is likely to be connected to the fact that our main bioink component relies on non-ionic polymer amphiphile. Again, optical images suggest a significant increase in cell number from day 1 to day 5. Consistently, DNA content in POx-*b*-POzi/Alg and POx-*b*-POzi/Alg/clay bioprinted samples were significantly increased from day 1 to day 5 (Figure 7b). The DNA content increased 1.6- fold at day 3 and about 2-fold at day 5 in POx-*b*-POzi/Alg and POx-*b*-POzi/Alg/clay. POx-*b*-POzi/Alg/clay exhibited a minor but statistically significant increase in DNA contents compared to POx-*b*-POzi/Alg group at day 5. Additionally, we evaluated viability of cells in POx-*b*-POzi/Alg/clay bioprinted samples at day 1 and day 5 using live/dead staining (Figure 7c). It is clearly apparent that the vast majority of cells were viable. In summary, the novel hybrid hydrogel bioink exhibited excellent cytocompatibility, bioprintability and structural stability, which may be opening new and improve paths to fabricate complex architectures whilst maintaining a cell-permissive environment. Although demonstrated at this point only for alginate, it should be obvious that this hybrid approach would be rather interesting for other bioink materials which may suffer from a less than optimal printability on their own.

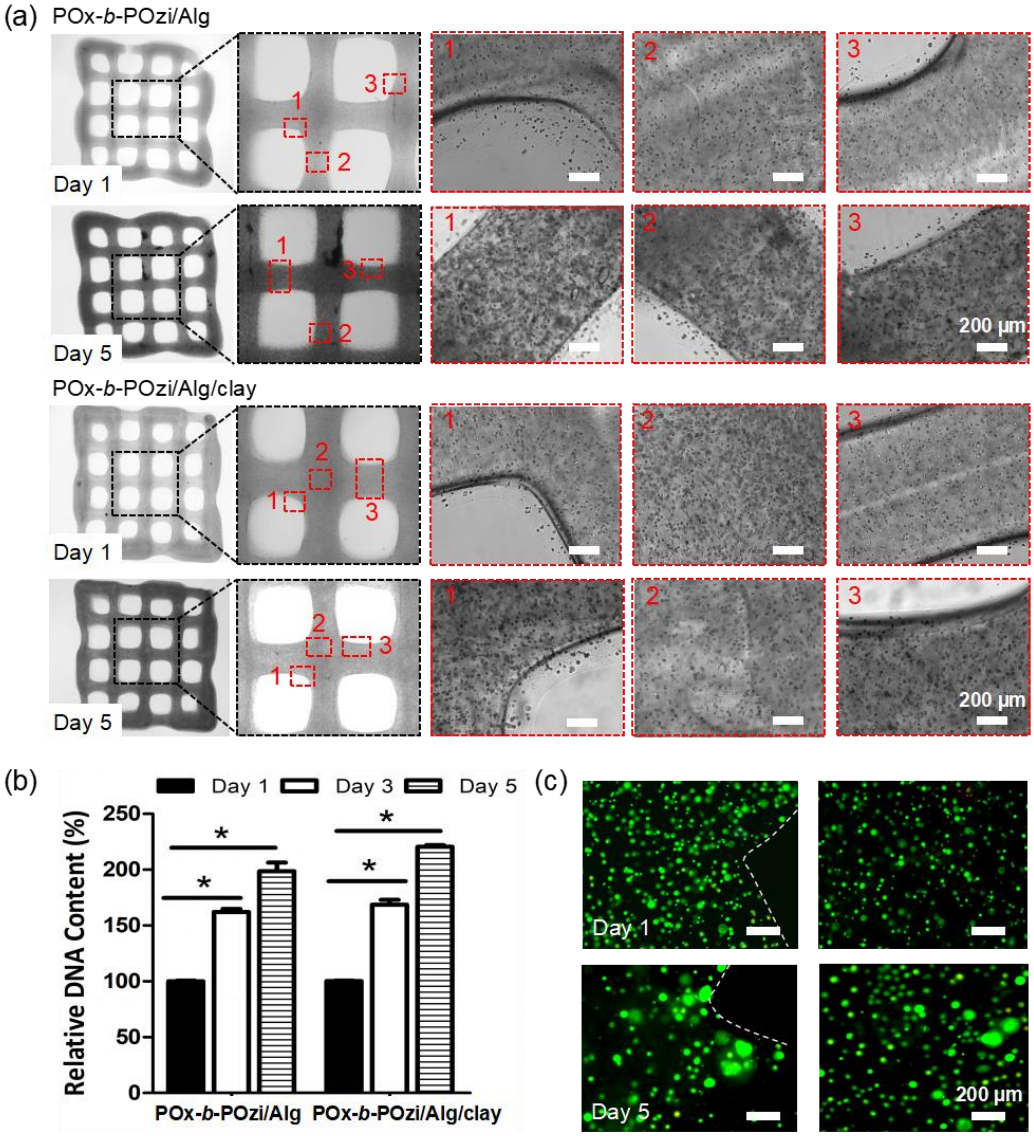

Figure 7. Cell (NIH 3T3 fibroblasts) distribution, proliferation, and viability in 3D bioprinted constructs. (a) Optical microscope images to visualize cell distribution at day 1 and day 5 in cell-laden 3D bioprinted 8-layer 5 x 5 line grids (12 × 12 mm) using POx-*b*-POzi/Alg and POx-*b*-POzi/Alg/clay bioinks, respectively. (b) DNA quantification within POx-*b*-POzi/Alg and POx-*b*-POzi/Alg/clay bioprinted construct (n=6) demonstrating cells proliferation at day 1, day 3, and day 5. (c) Live and dead staining in bioprinted constructs using POx-*b*-POzi/Alg/clay at day 1 and day 5. * indicate $p < 0.05$. All printing were carried out under an extrusion pressure of 100 kPa. Scale bar 200 µm in all images.

CONCLUSIONS

In this study, a novel advanced POx-*b*-POzi/Alg/clay hybrid hydrogel was introduced as a bioink for extrusion-based 3D bioprinting: A dual-step crosslinking approach was presented that exploited a primary thermogelling of the diblock copolymer

POx-*b*-POzi to achieve an improvement in rheological profiles beneficial for extrusion printing, while secondary ionic crosslinking with Ca^{2+} ions provided the long-term construct stabilization and mechanical flexibility. The excellent printability was demonstrated by various constructs printing with high stackability and shape fidelity and supported by a detailed rheological characterization. The post-printing ionic crosslinking of Alg polymer could also be realized by other di/trivalent cations, as exemplified by Fe^{3+} and Tb^{3+}. Additionally, the cell-laden printing and post-printing crosslinking process using Ca^{2+} ions was well tolerated by the embedded cells highlighting the feasibility of the novel hybrid hydrogels for 3D bioprinting. The presented hybrid approach, utilizing the beneficial properties of the POx-*b*-POzi base material should help to open new opportunities for the fabrication of complex architectures needed in the fields of tissue engineering and drug delivery.

ASSOCIATED CONTENT

Supporting Information

Detailed description of POx-*b*-POzi diblock copolymer synthesis and characterization; Compositions of the hydrogels studied in this work; The thermogelling properties of hydrogels; Ionic crosslinking time dependent gel content of the hydrogels; Applied shear stress dependent viscosity of the hydrogel precursor solutions at 37 °C; Dependence of G' and G'' on angular frequency for the hydrogels under different Ca^{2+} cross-linking time; Extrusion-based printing equipment; 3D printing of a 60-layer hollow cube; Cytocompatibility of the bioinks. (Figures S1−S6, Table S1) (PDF)

Sol-gel transition of the hydrogels (AVI)

Printability testing of the hydrogels (AVI)

3D printing of the POx-*b*-POzi/Alg/clay hybrid hydrogel (AVI)

AUTHOR INFORMATION

Corresponding Author

*E-mail: robert.luxenhofer@helsinki.fi

ORCID

Robert Luxenhofer: 0000-0001-5567-7404

Notes

RL is listed as inventor on a patent pertinent to some materials in the present work. The authors declare no other competing financial interest.

ACKNOWLEDGMENTS

The authors would like to gratefully acknowledge support by the Deutsche Forschungsgemeinschaft (DFG, German Research Foundation) – project number 326998133 – TRR 225 (subproject A03) awarded to R. Luxenhofer. C. Hu thanks China Scholarship Council (CSC) for the financial support. Furthermore, we thank the Deutsche Forschungsgemeinschaft for funding the crossbeam scanning electron microscope Zeiss CB 340 (INST 105022/58-1 FUGG) within the DFG State Major Instrumentation Programme. M. S. Haider is grateful to higher education commission of Pakistan and German academic exchange services (HEC-DAAD Pakistan) for the award of PhD scholarship. Alginate was received as a kind gift within the framework of the Transregio SFB TRR225 by J. Hazur (subproject A01, awarded to A. Boccaccini).

REFERENCES

(1) Murphy, S. V.; Atala, A. 3D Bioprinting of Tissues and Organs. *Nat. Biotechnol.* **2014,** *32*, 773-785.
(2) Mandrycky, C.; Wang, Z. J.; Kim, K.; Kim, D. H. 3D Bioprinting for Engineering Complex Tissues. *Biotechnol. Adv.* **2016,** *34*, 422-434.
(3) Duan, B. State-of-the-Art Review of 3D Bioprinting for Cardiovascular Tissue Engineering. *Ann. Biomed. Eng.* **2017,** *45*, 195-209.
(4) Pedde, R. D.; Mirani, B.; Navaei, A.; Styan, T.; Wong, S.; Mehrali, M.; Thakur, A.; Mohtaram, N. K.; Bayati, A.; Dolatshahi-Pirouz, A.; Nikkhah, M.; Willerth, S. M.; Akbari, M. Emerging Biofabrication Strategies for Engineering Complex Tissue Constructs. *Adv. Mater.* **2017,** *29*, 1606061.
(5) You, F.; Eames, B. F.; Chen, X. Application of Extrusion-Based Hydrogel Bioprinting for Cartilage Tissue Engineering. *Int. J. Mol. Sci.* **2017,** *18*, 1597.
(6) Malda, J.; Visser, J.; Melchels, F. P.; Jüngst, T.; Hennink, W. E.; Dhert, W. J. A.; Groll, J.; Hutmacher, D. W. 25th Anniversary Article: Engineering Hydrogels for Biofabrication. *Adv. Mater.* **2013,** *25*, 5011-5028.
(7) Ozbolat, I. T.; Hospodiuk, M. Current Advances and Future Perspectives in Extrusion-Based Bioprinting. *Biomaterials* **2016,** *76*, 321-343.
(8) Gungor-Ozkerim, P. S.; Inci, I.; Zhang, Y. S.; Khademhosseini, A.; Dokmeci, M. R. Bioinks for 3D Bioprinting: an Overview. *Biomater. Sci.* **2018,** *6*, 915-946.
(9) Placone, J. K.; Engler, A. J. Recent Advances in Extrusion-Based 3D Printing for Biomedical Applications. *Adv. Healthc. Mater.* **2018,** *7*, 1701101.

(10) Parak, A.; Pradeep, P.; du Toit, L. C.; Kumar, P.; Choonara, Y. E.; Pillay, V. Functionalizing Bioinks for 3D Bioprinting Applications. *Drug Discov. Today* **2019,** *24*, 198-205.
(11) Lee, K. Y.; Mooney, D. J. Alginate: Properties and Biomedical Applications. *Prog. polym. sci.* **2012,** *37*, 106-126.
(12) Jia, J.; Richards, D. J.; Pollard, S.; Tan, Y.; Rodriguez, J.; Visconti, R. P.; Trusk, T. C.; Yost, M. J.; Yao, H.; Markwald, R. R.; Mei, Y. Engineering Alginate as Bioink for Bioprinting. *Acta Biomater.* **2014,** *10*, 4323-4331.
(13) Jüngst, T.; Smolan, W.; Schacht, K.; Scheibel, T.; Groll, J. Strategies and Molecular Design Criteria for 3D Printable Hydrogels. *Chem. Rev.* **2016,** *116*, 1496-1539.
(14) Chimene, D.; Kaunas, R.; Gaharwar, A. K. Hydrogel Bioink Reinforcement for Additive Manufacturing: A Focused Review of Emerging Strategies. *Adv. Mater.* **2020,** *32*, e1902026.
(15) Faramarzi, N.; Yazdi, I. K.; Nabavinia, M.; Gemma, A.; Fanelli, A.; Caizzone, A.; Ptaszek, L. M.; Sinha, I.; Khademhosseini, A.; Ruskin, J. N.; Tamayol, A. Patient-Specific Bioinks for 3D Bioprinting of Tissue Engineering Scaffolds. *Adv. Healthc. Mater.* **2018,** *7*, e1701347.
(16) Li, H.; Tan, Y. J.; Leong, K. F.; Li, L. 3D Bioprinting of Highly Thixotropic Alginate/Methylcellulose Hydrogel with Strong Interface Bonding. *ACS Appl. Mater. Interfaces* **2017,** *9*, 20086-20097.
(17) Hazur, J.; Detsch, R.; Karakaya, E.; Kaschta, J.; Tessmar, J.; Schneidereit, D.; Friedrich, O.; Schubert, D. W.; Boccaccini, A. R. Improving Alginate Printability for Biofabrication: Establishment of a Universal and Homogeneous Pre-crosslinking Technique. *Biofabrication* **2020,** *12*, 045004.
(18) Ozbolat, I. T.; Chen, H.; Yu, Y. Development of 'Multi-Arm Bioprinter' for Hybrid Biofabrication of Tissue Engineering Constructs. *Robot. Com.-Int. Manuf.* **2014,** *30*, 295-304.
(19) Levato, R.; Jüngst, T.; Scheuring, R. G.; Blunk, T.; Groll, J.; Malda, J. From Shape to Function: The Next Step in Bioprinting. *Adv. Mater.* **2020,** *32*, 1906423.
(20) Hong, S. M.; Sycks, D.; Chan, H. F.; Lin, S. T.; Lopez, G. P.; Guilak, F.; Leong, K. W.; Zhao, X. H. 3D Printing of Highly Stretchable and Tough Hydrogels into Complex, Cellularized Structures. *Adv. Mater.* **2015,** *27*, 4035-4040.
(21) Dávila, J. L.; d'Ávila, M. A. Rheological Evaluation of Laponite/Alginate Inks for 3D Extrusion-Based Printing. *Int. J. Adv. Manuf. Tech.* **2018,** *101*, 675-686.
(22) Li, H.; Liu, S.; Lin, L. Rheological Study on 3D Printability of Alginate Hydrogel and Effect of Graphene Oxide. *International Journal of Bioprinting* **2016,** *2*, 54-66.
(23) Liu, S.; Bastola, A. K.; Li, L. A 3D Printable and Mechanically Robust Hydrogel Based on Alginate and Graphene Oxide. *ACS Appl. Mater. Interfaces* **2017,** *9*, 41473-41481.
(24) Leppiniemi, J.; Lahtinen, P.; Paajanen, A.; Mahlberg, R.; Metsa-Kortelainen, S.; Pinomaa, T.; Pajari, H.; Vikholm-Lundin, I.; Pursula, P.; Hytonen, V. P. 3D-Printable Bioactivated Nanocellulose-Alginate Hydrogels. *ACS Appl. Mater. Interfaces* **2017,** *9*, 21959-21970.

(25) Markstedt, K.; Mantas, A.; Tournier, I.; Martínez Ávila, H. c.; Hagg, D.; Gatenholm, P. 3D Bioprinting Human Chondrocytes with Nanocellulose–Alginate Bioink for Cartilage Tissue Engineering Applications. *Biomacromolecules* **2015,** *16*, 1489-1496.
(26) Bhattacharjee, T.; Zehnder, S. M.; Rowe, K. G.; Jain, S.; Nixon, R. M.; Sawyer, W. G.; Angelini, T. E. Writing in The Granular Gel Medium. *Sci. adv.* **2015,** *1*, e1500655.
(27) Hinton, T. J.; Jallerat, Q.; Palchesko, R. N.; Park, J. H.; Grodzicki, M. S.; Shue, H.-J.; Ramadan, M. H.; Hudson, A. R.; Feinberg, A. W. Three-Dimensional Printing of Complex Biological Structures by Freeform Reversible Embedding of Suspended Hydrogels. *Sci. adv.* **2015,** *1*, e1500758.
(28) Luxenhofer, R.; Schulz, A.; Roques, C.; Li, S.; Bronich, T. K.; Batrakova, E. V.; Jordan, R.; Kabanov, A. V. Doubly Amphiphilic Poly(2-oxazoline)s as High-Capacity Delivery Systems for Hydrophobic Drugs. *Biomaterials* **2010,** *31*, 4972-4979.
(29) Zhang, N.; Luxenhofer, R.; Jordan, R. Thermoresponsive Poly(2-Oxazoline) Molecular Brushes by Living Ionic Polymerization: Modulation of the Cloud Point by Random and Block Copolymer Pendant Chains. *Macromol. Chem. Phys.* **2012,** *213*, 1963-1969.
(30) Zahoranova, A.; Mrlik, M.; Tomanova, K.; Kronek, J.; Luxenhofer, R. ABA and BAB Triblock Copolymers Based on 2-Methyl-2-oxazoline and 2-n-Propyl-2-oxazoline: Synthesis and Thermoresponsive Behavior in Water. *Macromol. Chem. Phys.* **2017,** *218*, 1700031.
(31) Luxenhofer, R.; Han, Y.; Schulz, A.; Tong, J.; He, Z.; Kabanov, A. V.; Jordan, R. Poly(2-oxazoline)s as Polymer Therapeutics. *Macromol. Rapid Commun.* **2012,** *33*, 1613-31.
(32) Hartlieb, M.; Kempe, K.; Schubert, U. S. Covalently Cross-Linked Poly(2-oxazoline) Materials for Biomedical Applications-From Hydrogels to Self-Assembled and Templated Structures. *J. Mater. Chem. B* **2015,** *3*, 526-538.
(33) Dargaville, T. R.; Park, J. R.; Hoogenboom, R. Poly(2-oxazoline) Hydrogels: State-of-the-Art and Emerging Applications. *Macromol. Biosci.* **2018,** *18*, 1800070.
(34) Lorson, T.; Lübtow, M. M.; Wegener, E.; Haider, M. S.; Borova, S.; Nahm, D.; Jordan, R.; Sokolski-Papkov, M.; Kabanov, A. V.; Luxenhofer, R. Poly(2-oxazoline)s Based Biomaterials: A Comprehensive and Critical Update. *Biomaterials* **2018,** *178*, 204-280.
(35) Zahoranová, A.; Luxenhofer, R. Poly(2-oxazoline)- and Poly (2-oxazine)-Based Self-Assemblies, Polyplexes, and Drug Nanoformulations-An Update. *Adv. Healthc. Mater*. **2021**, *10*, 2001382.
(36) Lorson, T.; Jaksch, S.; Lübtow, M. M.; Jüngst, T.; Groll, J.; Lühmann, T.; Luxenhofer, R. A Thermogelling Supramolecular Hydrogel with Sponge-Like Morphology as a Cytocompatible Bioink. *Biomacromolecules* **2017,** *18*, 2161-2171.
(37) Monnery, B. D.; Hoogenboom, R. Thermoresponsive Hydrogels Formed by Poly(2-oxazoline) Triblock Copolymers. *Polym. Chem.* **2019,** *10*, 3480-3487.
(38) Lübtow, M. M.; Mrlik, M.; Hahn, L.; Altmann, A.; Beudert, M.; Lühmann, T.; Luxenhofer, R. Temperature-Dependent Rheological and Viscoelastic Investigation of a Poly(2-methyl-2-oxazoline)-b-poly(2-iso-butyl-2-oxazoline)-b-poly

(2-methyl-2-oxazoline)-Based Thermogelling Hydrogel. *J. Funct. Biomater.* **2019,** *10*, 36.
(39) Hu, C.; Hahn, L.; Yang, M.; Altmann, A.; Stahlhut, P.; Groll, J.; Luxenhofer, R. Improving Printability of A Thermoresponsive Hydrogel Biomaterial Ink by Nanoclay Addition. *J. Mater. Sci.* **2020,** *56*, 691-705.
(40) Haider M. S.; Ahmad T.; Yang, M.; Hu, C.; Hahn L.; Stahlhut, P.; Groll, J.; Luxenhofer, R. Tuning The Thermogelation and Rheology of Poly(2-oxazoline)/Poly(2-oxazine) Based Thermosensitive Hydrogels for 3D Bioprinting. *ChemRxiv.* **2021,** *DOI: 10.26434/chemrxiv.14472114*.
(41) Hahn, L.; Maier, M.; Stahlhut, P.; Beudert, M.; Flegler, V.; Forster, S.; Altmann, A.; Toppke, F.; Fischer, K.; Seiffert, S.; Bottcher, B.; Lühmann, T.; Luxenhofer, R. Inverse Thermogelation of Aqueous Triblock Copolymer Solutions into Macroporous Shear-Thinning 3D Printable Inks. *ACS Appl. Mater. Interfaces* **2020,** *12*, 12445-12456.
(42) Hahn, L.; Karakaya, E.; Zorn, T.; Sochor, B.; Maier, M.; Stahlhut, P.; Forster, S.; Fischer, K.; Seiffert, S.; Pöppler, A.-C.; Detsch R.; Luxenhofer R. An Inverse Thermogelling Bioink Based on an ABA Type Poly (2-Oxazoline) Amphiphile. *ChemRxiv.* **2021,** *DOI: 10.26434/chemrxiv.14317205.v1*.
(43) Hahn, L.; Keßler, L.; Polzin, L.; Fritze, L.; Helten, H.; Luxenhofer, R. ABA Type Amphiphiles with Poly (2-Benzhydryl-2-Oxazine) Moieties: Synthesis, Characterization and Inverse Thermogelation. *ChemRxiv.* **2021,** *DOI: 10.26434/chemrxiv.14322194.v1*.
(44) Gauvin-Rossignol, G.; Legros, P.; Ruel, J.; Fortin, M. A.; Begin-Drolet, A. Sugar Glass Fugitive Ink Loaded with Calcium Chloride for The Rapid Casting of Alginate Scaffold Designs. *Heliyon* **2018,** *4*, e00680.
(45) Kolesky, D. B.; Truby, R. L.; Gladman, A. S.; Busbee, T. A.; Homan, K. A.; Lewis, J. A. 3D Bioprinting of Vascularized, Heterogeneous Cell-Laden Tissue Constructs. *Adv. Mater.* **2014,** *26*, 3124-3130.
(46) Haigh, J. N.; Chuang, Y. M.; Farrugia, B.; Hoogenboom, R.; Dalton, P. D.; Dargaville, T. R. Hierarchically Structured Porous Poly(2-oxazoline) Hydrogels. *Macromol. Rapid Commun.* **2016,** *37*, 93-99.
(47) Sinnwell, S.; Ritter, H. Microwave Accelerated Polymerization of 2-phenyl-5,6-dihydro-4H-1,3-oxazine: Kinetics and Influence of End-Groups on Glass Transition Temperature. *Macromol. Rapid Commun.* **2006,** *27*, 1335-1340.
(48) Jin, Y. F.; Liu, C. C.; Chai, W. X.; Compaan, A.; Huang, Y. Self-Supporting Nanoclay as Internal Scaffold Material for Direct Printing of Soft Hydrogel Composite Structures in Air. *ACS Appl. Mater. Interfaces* **2017,** *9*, 17457-17466.
(49) Paxton, N.; Smolan, W.; Bock, T.; Melchels, F.; Groll, J.; Jüngst, T. Proposal to Assess Printability of Bioinks for Extrusion-Based Bioprinting and Evaluation of Rheological Properties Governing Bioprintability. *Biofabrication* **2017,** *9*, 044107.
(50) Schwab, A.; Levato, R.; D'Este, M.; Piluso, S.; Eglin, D.; Malda, J. Printability and Shape Fidelity of Bioinks in 3D Bioprinting. *Chem. Rev.* **2020,** *120,* 11028-11055.
(51) Mignon, A.; Pezzoli, D.; Prouve, E.; Levesque, L.; Arslan, A.; Pien, N.; Schaubroeck, D.; Van Hoorick, J.; Mantovani, D.; Van Vlierberghe, S.; Dubruel, P. Combined Effect of

Laponite and Polymer Molecular Weight on The Cell-Interactive Properties of Synthetic PEO-Based Hydrogels. *React. Funct. Polym.* **2019,** *136*, 95-106.
(52) Chimene, D.; Peak, C. W.; Gentry, J. L.; Carrow, J. K.; Cross, L. M.; Mondragon, E.; Cardoso, G. B.; Kaunas, R.; Gaharwar, A. K. Nanoengineered Ionic-Covalent Entanglement (NICE) Bioinks for 3D Bioprinting. *ACS Appl. Mater. Interfaces* **2018,** *10*, 9957-9968.
(53) Murugesan, S.; Scheibel, T. Copolymer/Clay Nanocomposites for Biomedical Applications. *Adv. Funct. Mater.* **2020,** *30*, 1908101.
(54) Ribeiro, A.; Blokzijl, M. M.; Levato, R.; Visser, C. W.; Castilho, M.; Hennink, W. E.; Vermonden, T.; Malda, J. Assessing Bioink Shape Fidelity to Aid Material Development in 3D Bioprinting. *Biofabrication* **2017,** *10*, 014102.

Supporting Information

A Thermogelling Organic-Inorganic Hybrid Hydrogel with Excellent Printability, Shape Fidelity and Cytocompatibility for 3D Bioprinting

Chen Hu,[†] Taufiq Ahmad,[‡] Malik Salman Haider,[†] Lukas Hahn,[†] Philipp Stahlhut,[‡] Jürgen Groll,[‡] and Robert Luxenhofer[†, §, *]

[†]Functional Polymer Materials, Chair for Advanced Materials Synthesis, Institute for Functional Materials and Biofabrication, Department of Chemistry and Pharmacy, Julius-Maximilians-University Würzburg, Röntgenring 11, 97070 Würzburg, Germany
[‡]Department of Functional Materials in Medicine and Dentistry, Institute for Functional Materials and Biofabrication and, Bavarian Polymer Institute, Julius-Maximilians-University Würzburg, Pleicherwall 2, 97070 Würzburg, Germany
[§]Soft Matter Chemistry, Department of Chemistry and Helsinki Institute of Sustainability Science, Faculty of Science, University of Helsinki, PB 55, 00014 Helsinki, Finland

***Corresponding author:** robert.luxenhofer@helsinki.fi

(a)

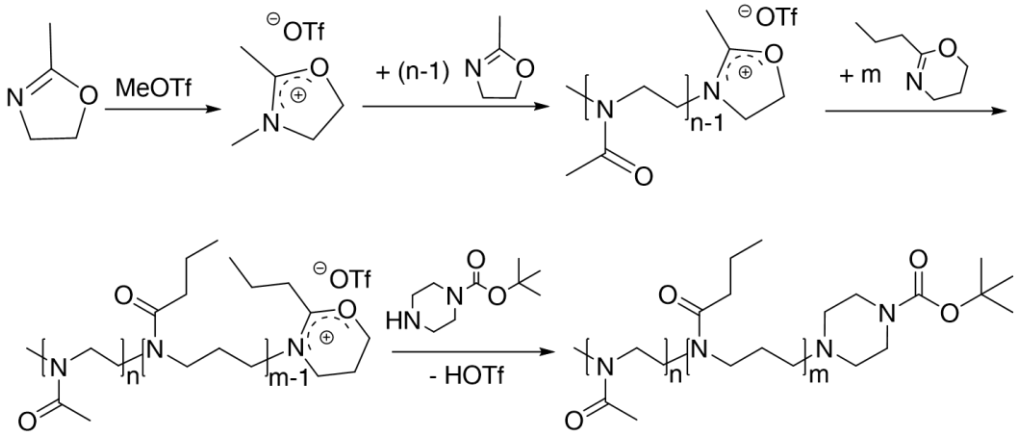
MeOTf
OTf
+ (n-1)
n-1
+ m
m-1
HN
- HOTf
n
m

(b)

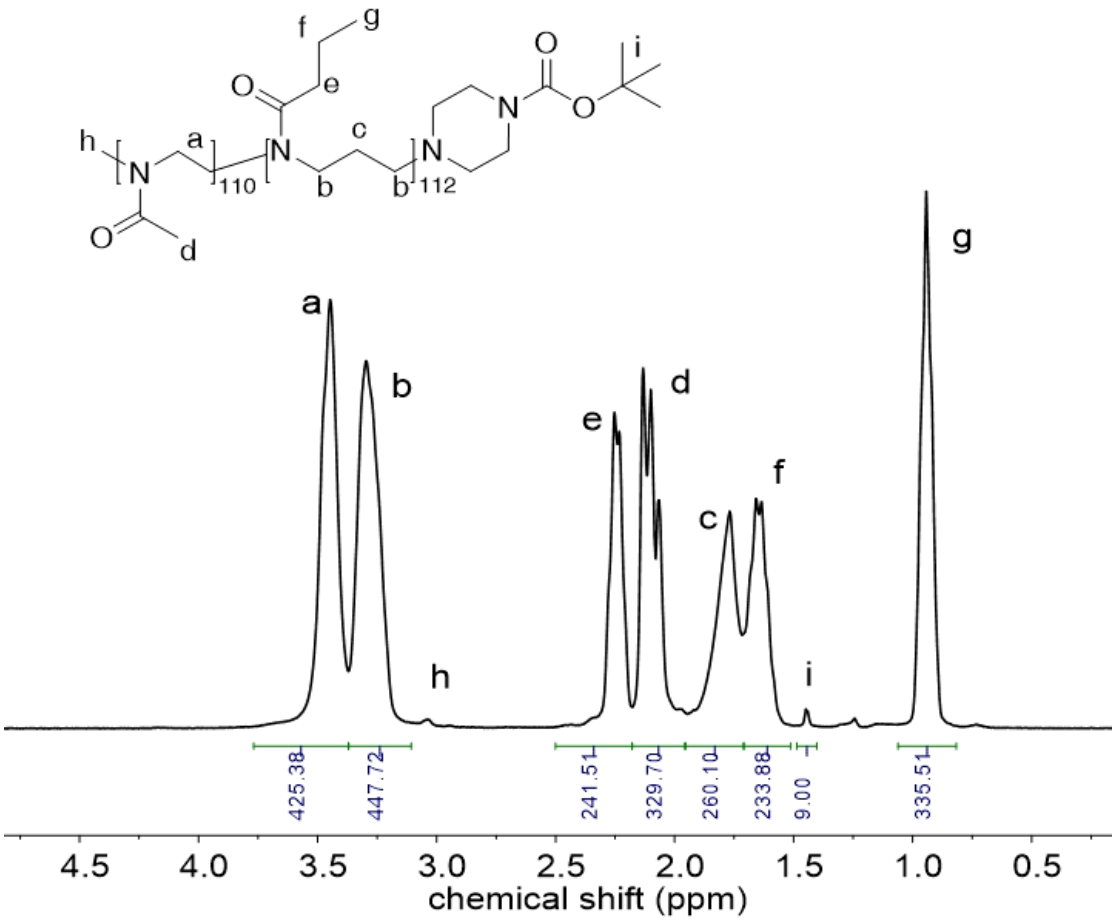
a
b
h
e
d
c
f
i
g
425.38
447.72
241.51
329.70
260.10
233.88
9.00
335.51
4.5
4.0
3.5
3.0
2.5
2.0
1.5
1.0
0.5
chemical shift (ppm)

(c)

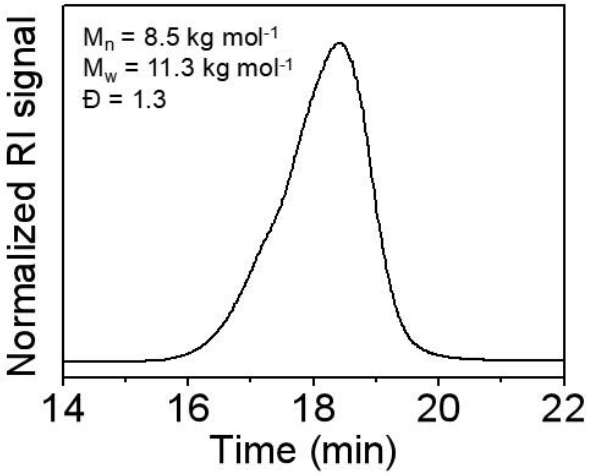

Figure S1: (a) Synthesis of the diblock copolymer POx-*b*-POzi *via* living cationic ring opening polymerization of 2-*n*-propyl-oxazine (nPrOzi) and 2-methyl-2-oxazoline (MeOx) monomers. Methyl triflate (MeOTf) was used as initiator and 1-Boc-piperazine as terminating agent. (b) Chemical structure of the synthesized diblock copolymer POx-*b*-POzi and the corresponding ^{1}H NMR spectrum ($CDCl_3$; 300 MHz; 298 K). From the signals in the ^{1}H NMR spectrum with chemical shifts at 2.10 ppm (CH_3 of PMeOx) and 0.94 ppm (CH_3 of PnPrOzi), the relative block lengths and diblock copolymer composition was determined to be POx_{110}-*b*-$POzi_{112}$. (c) GPC profile of the diblock POx-*b*-POzi diblock copolymer (with HFIP as eluent).

Table S1: Compositions of the hydrogels studied in this work.*

sample	compositions (% w/w)		
	POx-*b*-POzi	Alg	clay
POx-*b*-POzi/Alg	**20**	**1**	**-**
POx-*b*-POzi/Alg	20	2	-
POx-*b*-POzi/Alg	20	3	-
POx-*b*-POzi/Alg/clay	**20**	**1**	**1.5**

* Post-crosslinking by 1 wt% (0.09 mol L^{-1}) $CaCl_2$, or 0.3 mol L^{-1} $FeCl3{\cdot}6H_2O$ or 0.3 mol L^{-1} $TbCl_3{\cdot}6H_2O$ accordingly. Dyed by carmine in where needed.

* Unless otherwise noted, the POx-*b*-POzi/Alg (20/1 wt%) and POx-*b*-POzi/Alg/clay (20/1/1.5 wt%) hydrogels which were marked in bold were used for further study.

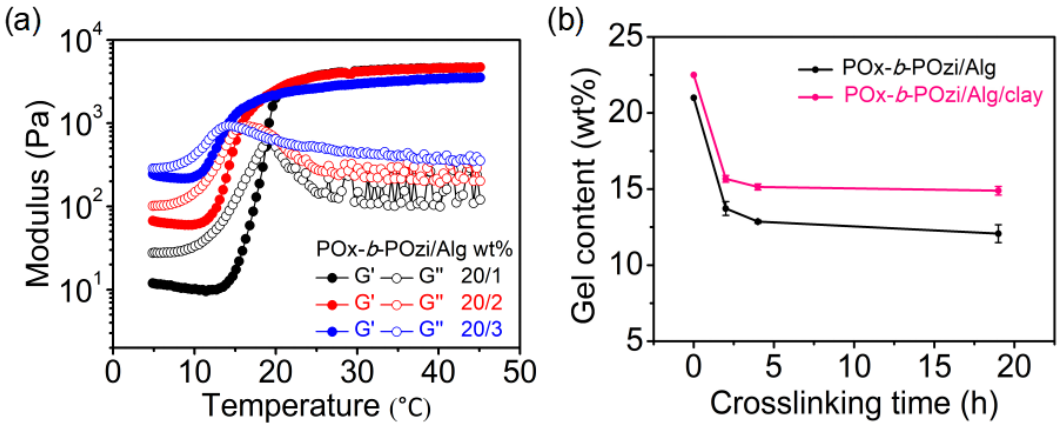

Figure S2: (a) Thermogelling property of the POx-*b*-POzi/Alg hydrogel precursor solutions with a constant POx-*b*-POzi concentration of 20 wt% and various Alg concentration from 1 to 3 wt%. (b) Ionic crosslinking time dependent gel content of the hydrogels.

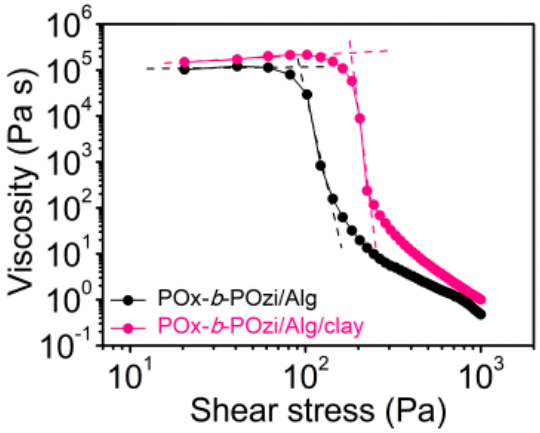

Figure S3: Applied shear stress dependent viscosity of the hydrogel precursor solutions at 37 °C. The intersection of dashed lines is commonly referred to as the yield point.

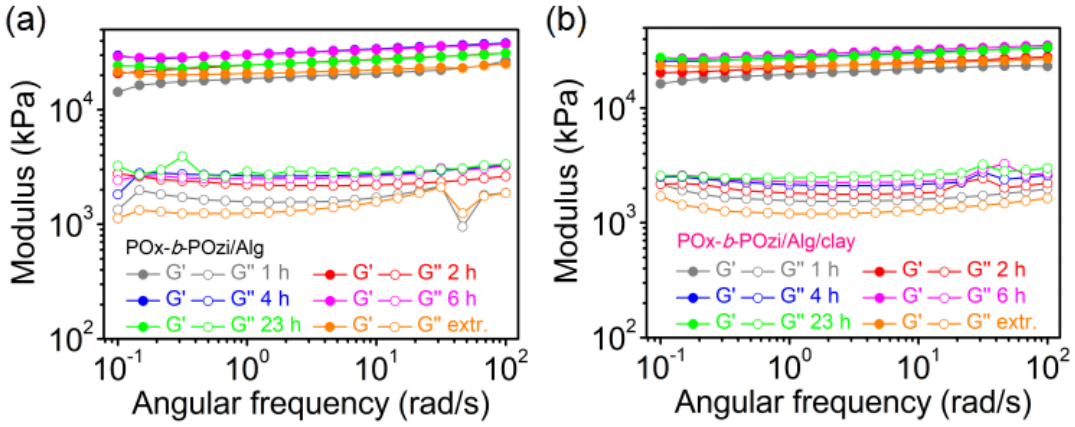

Figure S4: Dependence of G' and G'' on angular frequency for POx-*b*-POzi/Alg (a) and POx-*b*-POzi/Alg/clay (b) hydrogels under different Ca^{2+} cross-linking time.

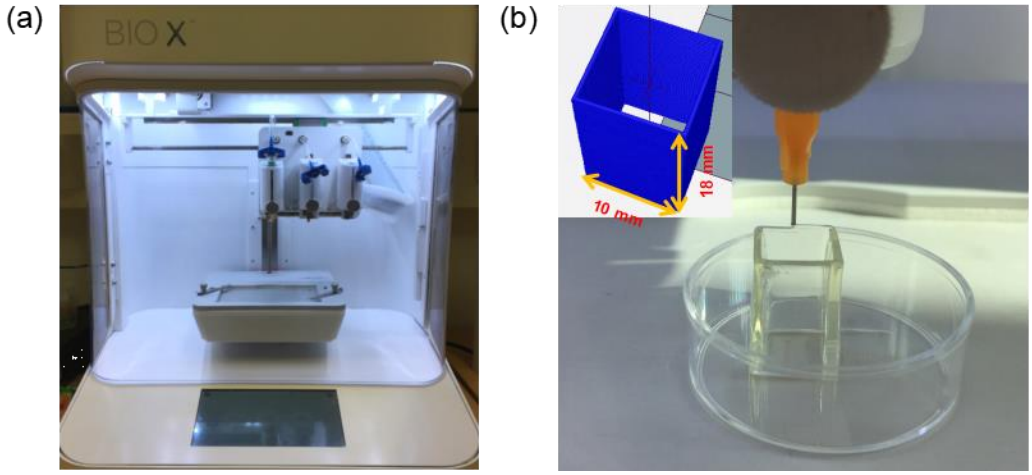

Figure S5: (a) Extrusion-based printer used in this study. (b) 3D printing of a 60-layer hollow cube with POx-*b*-POzi/Alg/clay hydrogel ink.

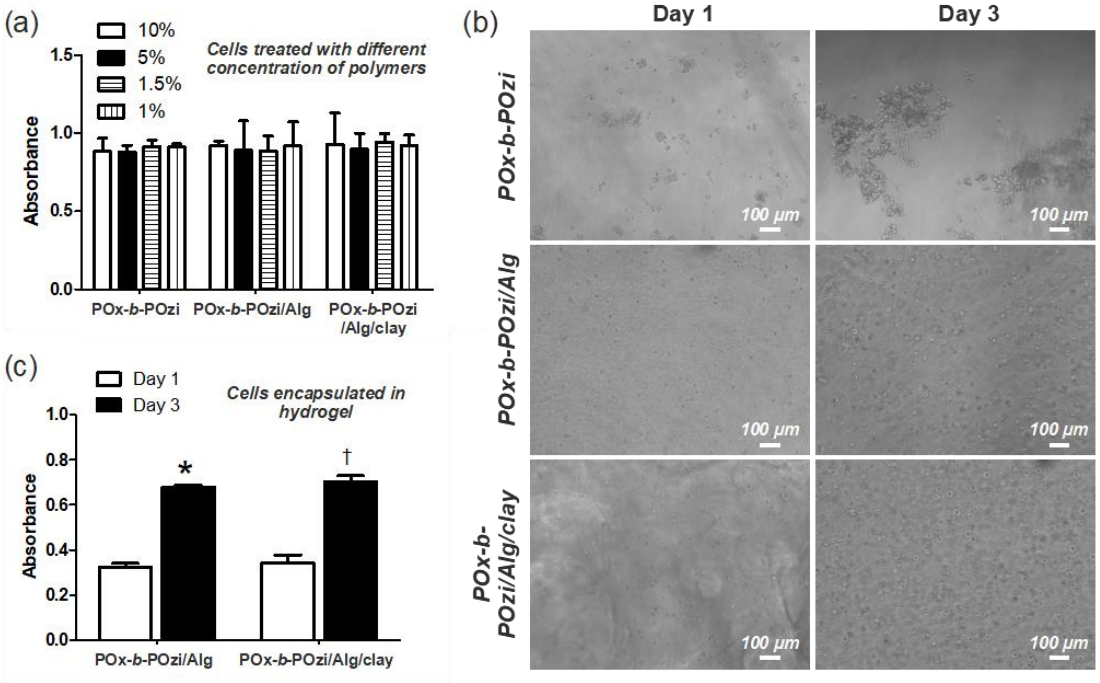

Figure S6: Cytocompatibility of bioink. (a) WST-1 assay of fibroblast treated with different concentrations of POx-*b*-POzi, POx-*b*-POzi/Alg and POx-*b*-POzi/Alg/clay in growth media (n=4). (b) Optical microscope images of cell-laden POx-*b*-POzi, POx-*b*-POzi/Alg, and POx-*b*-POzi/Alg/clay hydrogels. (c) WST-1 assay of cell-laden POx-*b*-POzi/Alg and POx-*b*-POzi/Alg/clay (n=4). * and † indicates $P < 0.05$ compared to POx-*b*-POzi/Alg at day 1 and POx-*b*-POzi/Alg/clay at day 1, respectively.

Video S1: The reversible sol-gel transition of the hydrogels (AVI)

Video S2: Printability testing of the hydrogels (AVI)

Video S3: 3D printing of the POx-*b*-POzi/Alg/clay hybrid hydrogel (AVI)